Author Manuscript

Author Manuscript

Author Manuscript

Author Manuscript

HHS Public Access

Author manuscript

Nat Neurosci. Author manuscript; available in PMC 2012 July 01.

Published in final edited form as:

Nat Neurosci. ; 15(1): 123–130. doi:10.1038/nn.2984.

Novel GABAergic circuits mediate the reinforcement-related signals of striatal cholinergic interneurons

Daniel F. English[1], **Osvaldo Ibanez-Sandoval**[1], **Eran Stark**[1], **Fatuel Tecuapetla**[1,†], **Gyorgy Buzsaki**[1], **Karl Deisseroth**[2], **James M. Tepper**[1], and **Tibor Koos**[1]

[1]Center for Molecular and Behavioral Neuroscience, Rutgers University, Newark, NJ 07102

[2]Department of Bioengineering, Stanford University, Stanford, CA 94305

Abstract

Neostriatal cholinergic interneurons are believed to play an important role in reinforcement mediated learning and response selection by signaling the occurrence and motivational value of behaviorally relevant stimuli through precisely timed multiphasic population responses. An important problem is to understand how these signals regulate the functioning of the neostriatum. Here we describe the synaptic organization of a novel circuit that involves direct nicotinic excitation of GABAergic interneurons and enables cholinergic interneurons to exert rapid inhibitory control of the activity of projection neurons. We also demonstrate that the dominant effect of an optogenetically reproduced pause-excitation population response of cholinergic interneurons is powerful and rapid inhibition of the firing of projection neurons that is coincident with synchronous cholinergic activation. These results reveal a previously unknown circuit mechanism that transmits reinforcement-related information of ChAT interneurons in the mouse neostriatal network.

The neostriatum plays a critical role in the reinforcement mediated acquisition and selection of adaptive behavioral responses[1,2]. These functions require neuronal representation of information about the occurrence and motivational value of external stimuli that are provided by 2 major neuromodulatory systems, midbrain dopaminergic neurons, and local cholinergic (ChAT) interneurons. These 2 neuron populations exhibit coincident firing rate changes in response to the presentation of unpredicted or the omission of predicted primary

Users may view, print, copy, download and text and data- mine the content in such documents, for the purposes of academic research, subject always to the full Conditions of use: http://www.nature.com/authors/editorial_policies/license.html#terms

Correspondence should be addressed to Tibor Koos, Ph.D., Center for Molecular and Behavioral Neuroscience, Rutgers University, 197 University Avenue Newark, NJ 07102, Tel: 973.353.1080 × 3634, Fax: 973.353.1588 tibkoos@yahoo.com.
Present Address: Neurobiology of Action, Instituto Gulbenkian de Ciencia, Rua da Quinta Grande, 6, 2780-156 Oeiras, Portugal

Author Contributions. D.E. carried out all *in vivo* recording experiments and data analysis and performed the majority of the *in vitro* experiments, contributed to virus production, virus injections and confocal imaging (with the exception of Fig. 1a, obtained by Dr. J. Berlin). O.I. and F.T. performed the initial *in vitro* analysis of NPY-NGF neurons and O.I. first identified nicotinic synapses in these interneurons. E.S. contributed to the design of *in vivo* recording and optical stimulation methods and data analysis, molecular biology and virus production. G.B. contributed to optrode design and the design and analysis of *in vivo* recording experiments. K.D. designed and provided constructs for optogenetic expression vectors, designed and produced the *AAV5-DIO-eNpHR3.0-YFP* and the *AAV5-DIO-ChR2-mCherry* virus vectors and contributed to optogenetic methods. J.M.T. contributed to the development of *in vitro* and *in vivo* recording methods. T.K. performed *in vitro* recordings, recombinant DNA procedures and lentivirus production. The study was designed by T.K., J.M.T and D.E. and the manuscript was written by T.K. with significant contribution from D.E. and J.M.T. reflecting input from all authors.

Author Manuscript Author Manuscript Author Manuscript Author Manuscript

reinforcement, as well as to cues predictive of these stimuli and together encode the value, magnitude and expectation probability of these events[2-8]. In particular, ChAT interneurons exhibit multiphasic population responses which consist of a brief (200-300 ms) cessation of firing, termed the pause response and, depending on the nature of the stimulus and its behavioral context, an immediately following and sometimes a preceding period of brief semi-synchronous excitation[3,4,6-9]. An important question is to elucidate how these population responses regulate the functioning of the neostriatal network. Due to the multiphasic nature of these responses and the absence of spatial segregation of ChAT interneurons classical methods have not been adequate to address this issue. Here we used optogenetic excitatory and inhibitory tools to reproduce synchronous excitation and pause-excitation firing patterns of ChAT interneurons and demonstrate that ChAT interneurons activate parallel GABAergic circuits that mediate powerful inhibition of striatal projection neurons *in vitro* as well as *in vivo*.

Results

Cholinergic interneurons activate GABAergic inhibition in SPNs

All experiments were conducted with the approval of the *Rutgers University Institutional Animal Care and Use Committee*. The effects of synchronous activation of ChAT interneurons were examined using Channelrhodopsin-2 (ChR2-YFP) expressed in ChAT interneurons with viral mediated transfer of a Cre-lox controlled transgene. ChR2 expression specificity was verified with immunocytochemistry demonstrating ChAT expression in ∼98.7% (81/82) of ChR2-YFP$^+$ neurons (Fig. 1a). Postsynaptic responses to activation of cholinergic interneurons (Fig. 1b) were investigated *in vitro* in brains slices prepared from adult (PD 60-390) mice using standard methods[10]. In all SPNs examined, (n=94), synchronous activation of ChAT interneurons elicited a polysynaptic $GABA_A$ receptor mediated inhibitory postsynaptic potential/current (IPSP/IPSC, Fig. 1c, d) involving nicotinic receptors, because the response was blocked by selective antagonists of $GABA_A$ and Type-2 nicotinic receptors (bicuculline, 10 μM, n=10, and dihydro-β-erythroidine, DHβE, 100 nM-10 μM, n=10, respectively, Fig. 1d), but not by antagonists of AMPA-type glutamatergic receptors (CNQX, 10 μM, n=10, Supplementary Fig. 1) or muscarinic receptors (atropine, 10 μM, n=3, not shown). The IPSC was characterized by a relatively long onset-latency and short rise-time (11±1.7 ms and 5.0±0.6 ms, respectively, n=11), and exhibited a peak conductance of 2.8±0.9 nS. In current clamp, optical stimulation elicited large amplitude IPSPs in SPNs (n=20) that efficiently blocked action potential generation and decreased the momentary firing rate of projection neurons in a rate dependent manner (Fig. 1c, Supplementary Fig. 2). We also investigated the contribution of single ChAT interneurons to the inhibition of SPNs using paired recordings. In ∼50% of pairs, (n=21), single spikes in ChAT interneurons elicited bicuculline (10 μM, n=4) and DHβE (10 μM, n=3) sensitive small IPSCs in SPNs (<20 pA, CsCl internal solution, E[Cl]∼=-10 mV, Supplementary Fig. 3).

The GABAergic inhibition in SPNs involves multiple biophysically distinct mechanisms

The optically elicited IPSCs in SPNs were multiphasic consisting of 3 kinetically distinct phases characterized by τ_{decay} values of 5.2±1.8 ms, 96±11.7 ms and 906±106 ms (n=6).

Author Manuscript Author Manuscript Author Manuscript Author Manuscript

Henceforth, we will refer to the first 2 components as fast and slow IPSCs (fIPSC, and sIPSC, Fig. 1e). Due to its small amplitude (~20 pA) the mechanism underlying the slowest component was not investigated further. In about 1/3 of the SPNs the transition between these response components was not monotonic but the sIPSC was introduced by a clear inflection (Fig. 1e) suggesting that the compound response represents the superposition of 2 distinct GABAergic responses, a typical fast IPSC and a slowly rising and slowly decaying GABAergic response, that was less apparent when the onset of the sIPSC was obscured by larger or slower fIPSC components (Fig. 1e, inset). To test more directly the involvement of 2 distinct mechanisms we examined the trial-to-trial correlation of the amplitudes of the fIPSC and sIPSC components (Fig. 1f). Close examination of individual responses and linear regression analysis demonstrated that the amplitude of the fIPSC and the sIPSC varied independently (Fig. 1f). This excluded the possibility that the sIPSC represented a distinct kinetic phase of activation of the same receptors that mediate the fIPSC or that the 2 responses were secondary to the release of GABA from the same axon terminals reaching functionally distinct receptor populations.

We also noted that the sIPSC appeared similar to a form of slow $GABA_A$ receptor mediated inhibition ($GABA_A$-slow) first described in the hippocampus and the neocortex[11-13]. To test the possibility that the sIPSC involved a similar mechanism we took advantage of the characteristic sensitive dependence of the τ_{decay} of this response on inhibition of GABA transport[14-16], a characteristic not exhibited by conventional GABAergic synapses[16,17]. Application of NO711 (10 μM) a selective inhibitor of GAT-1 dramatically increased the τ_{decay} of the sIPSC from 57.5±2.5 ms to 185.2±17.5 ms (322%, n=4, Wilcoxon test, p=0.02, Fig. 1g). In contrast, the time course of the fIPSC was not affected (Fig. 1g, Control: 10.5±1.7 ms, NO711: 9.3±4.9 ms; n=3, p=0.6, Wilcoxon test). Together these results demonstrated that the fIPSC and the sIPSC originate from separate and biophysically distinct mechanism including a component that resembles $GABA_A$-slow.

NPY-NGF neurons give rise to the sIPSC component of inhibition in SPNs

We have recently demonstrated the existence of a class of neuropeptide Y (NPY) expressing interneurons in the neostriatum, the NPY-neurogliaform (NPY-NGF interneurons) that are morphologically and electrophysiologically distinct from the previously known NPY expressing, plateau depolarization-low threshold spike (NPY-PLTS) neurons[18]. Importantly, unlike NPY-PLTS neurons that very rarely contact SPNs,[19] NPY-NGF interneurons elicit an IPSC in most nearby SPNs (~84%) that is kinetically very similar to $GABA_A$-slow[18]. The comparative properties of NPY-NGF and NPY-PLTS interneurons are illustrated in Supplementary Fig. 4 and 5. Interestingly, in addition to eliciting a slow GABAergic IPSC these interneurons exhibit striking electrophysiological and morphological similarity to NPY expressing neurogliaform neurons in the neocortex[15] and hippocampus[14] that are the primary source of $GABA_A$-slow in these brain areas[20].

We thus hypothesized that NPY-NGF interneurons may be responsible for the sIPSC component in SPNs. To examine this possibility we first obtained triple and paired recordings to test if NPY-NGF interneurons received nicotinic synaptic excitation from ChAT interneurons and whether the same NPY-NGF interneurons elicited IPSCs similar to

Author Manuscript Author Manuscript Author Manuscript Author Manuscript

the sIPSC component in SPNs using NPY-EGFP transgenic reporter mice (Fig. 2a). In 8 of 14 instances of simultaneously recorded ChAT and NPY-NGF interneurons (n=8 of ChAT, NPY-NGF, SPN triples and n=6 pairs) a postsynaptic response could be elicited in the NPY-NGF neurons by single action potentials in the ChAT interneuron (57% connectivity, Fig. 2b). While in most cases the ChAT interneurons were activated in voltage clamp action potentials triggered in current clamp elicited similar postsynaptic responses (Supplementary Fig. 6). The response had an average amplitude of 0.96±0.7 mV, (range: 0.28-2.27 mV), rise time of 14.7±5.3 ms, (range: 9.0-24.7 ms), decay time constant of 75.6±40.2 ms, (range: 27.8-147 ms), onset latency of 3.6±1.6 ms and exhibited no transmission failures (Fig. 2b). The response was a Type-2 receptor mediated nicotinic postsynaptic excitatory potential (nEPSP) because it was blocked by DHβE (200 nM, n=3; 1 μM, n=2; Fig. 2b) but not by glutamatergic AMPA or $GABA_A$ receptor antagonists (CNQX, 10 μM, n=3; bicuculline, 10 μM, n=4; not shown). Stimulation of ChAT interneurons also triggered recurrent IPSCs (Fig. 2c). Train stimulation (n=2; 3.33 Hz, 3 spikes) revealed significant but incomplete depression of the nEPSP (60-75%, n=2, Fig. 2d) that contrasted the complete use-dependent suppression of recurrent GABAergic inhibition in simultaneously recorded ChAT interneurons (Fig. 2d). Among the 8 NPY-NGF interneurons shown to receive nicotinic innervation from a ChAT interneuron 4 out of 5 tested interneurons elicited IPSCs in SPNs (Fig. 2e). The IPSC elicited by NPY-NGF interneurons in SPNs (n=11, 4 from triple recordings and 7 in additional pairs) was similar to $GABA_A$-slow and exhibited an average amplitude of 155.7±160.7 pA, (range: 17.6-534 pA), rise time of 9.5±4.9 ms, (range: 3.6-17.8 ms), τ_{decay} of 65.8±14.98 ms, (range: 37-93 ms; CsCl internal solution, Fig. 2e, f, Supplementary Fig. 5). The probability of connectivity to SPNs was very high 11/14 (78 %). The τ_{decay} of the IPSC (68.7±12.1 ms, range: 56-93 ms) did not differ significantly from the τ_{decay} of the sIPSC in SPNs elicited with optogenetic stimulation of ChAT interneurons (96±28.7 ms, Wilcoxon test, $p>0.05$, n=6). Importantly, the IPSCs elicited by NPY-NGF interneurons never included fast IPSC components or exhibited biphasic decay (Fig. 2e, f, Supplementary Fig. 5).

To further test the contribution of NPY-NGF interneurons to the sIPSC we next tested the effect of GAT-1 inhibition. NO711 increased the τ_{decay} of the IPSC in a dose dependent manner from 61.3±9.2 ms to 205.6±28 ms at 10 μM (336%, n=3, Fig. 2f) and from 92±28.3 ms to 1310±975 ms at 50 μM (not shown, n=2, p=0.02, Wilcoxon test, n=5 total). The effects of NO711 on the optogenetic sIPSC and the IPSC elicited by NPY-NGF neurons were essentially identical at the same drug concentration (322% vs. 336%, Fig. 2f).

In addition, we observed that in 3/14 pairs (21 %), NPY-NGF interneurons elicited a GABAergic IPSC in ChAT interneurons (Fig. 2e). This response was blocked by bicuculline (n=2, Fig. 2e) and exhibited small amplitudes (9.4±8 pA; range: 2.8-18.5 pA, $E[Cl^-]\sim=-10$ mV). Importantly, NPY-NGF neurons could not mediate recurrent inhibition of ChAT interneurons because this IPSC and the recurrent IPSCs exhibited very different τ_{decay} values (77±37 ms, n=3 vs. 19.2±12.7 ms, n=8, respectively; p=0.014, Wilcoxon test; Fig. 2c, e) and because activation of single ChAT interneurons never elicited action potentials or nEPSPs approaching spike threshold in NPY-NGF neurons although recurrent inhibition was frequently triggered (Fig. 2c, Supplementary Fig. 7). Finally, electrotonic coupling was also observed in 1 of 2 pairs of NPY-NGF interneurons (Supplementary Fig. 5).

Author Manuscript Author Manuscript Author Manuscript Author Manuscript

These observations demonstrate the existence of a highly interconnected circuitry between ChAT and NPY-NGF interneurons and SPNs in which NPY-NGF neurons receive dense cholinergic excitatory input from ChAT interneurons and provide widespread innervation of SPNs using slow GABAergic inhibition.

We next tested if synchronous activation of ChAT interneurons elicited action potentials in NPY-NGF interneurons using slices from double transgenic *ChAT-Cre/NPY-EGFP* mice that allowed selective optogenetic stimulation of ChAT interneurons using targeted ChR2 expression and visualized recording from NPY-NGF neurons (Fig. 3a, b). Optogenetic stimulation of the ChAT interneuron population elicited large amplitude depolarizing postsynaptic potentials in all NPY-NGF neurons tested, and in 2 of 7 neurons triggered 1-3 action potentials with interspike intervals < 10 ms. (Fig. 3c-e). Simultaneous recordings from nearby SPNs (n=3) demonstrated that the postsynaptic responses in the NPY-NGF neurons were accompanied by compound optogenetic IPSCs in the SPNs and that the same NPY-NGF neurons themselves elicited slow $GABA_A$ receptor mediated responses in the projection neurons (Fig. 3c). Reversal potential measurements revealed that the optogenetically elicited postsynaptic response in NPY-NGF interneurons consisted of an early excitatory and a delayed inhibitory component (Fig. 3d). The IPSC component, which itself was secondary to nicotinic receptor activation (not shown), exhibited 4-12 mV amplitudes (V_m∼-45 mV, E[Cl]∼-69 mV) and was $GABA_A$ receptor mediated (bicuculline, 10 μM, n=5, Fig. 3d, e). This inhibitory response may play an important role in limiting the nicotinic activation of NPY-NGF neurons because in 1 cell that did not fire action potentials in control medium firing was elicited after $GABA_A$ receptor block (Fig. 3e). The pharmacologically isolated excitatory response (n=5) was a nEPSP because it was reduced in amplitude by >95% by DHβE both at 200 nM (n=2) and at 1 μM (n=3, Fig. 3c, e). The nEPSP exhibited amplitudes of 8.8-34.2 mV (average: 16.8 mV±10.3 mV), rise time of 16.8±2.2 ms (range: 16.5-21.5 ms), and τ_{decay} of 60.0±8.9 ms, (range: 51-71 ms, Fig. 3e). No contribution from glutamatergic AMPA receptors was detected (Fig. 3e).

FS interneurons and NPY-PLTS interneurons are not involved in the GABAergic responses elicited by ChAT interneurons

Other neostriatal interneuron types were tested to see if they could mediate the fIPSC and/or contribute to the sIPSC component of the compound optogenetic IPSC in SPNs. SPNs themselves could be excluded because they lack nicotinic receptors[21] and were not activated in optogenetic experiments (Fig. 1c). Fast spiking interneurons (FSI) are another major source of inhibition of SPNs[22] (Fig. 4a) and represent an important candidate because they express nicotinic receptors[23] and receive cholinergic innervation[24]. Cholinergic stimulation failed to elicit significant depolarization (>3 mV) or action potential firing in the recorded FSIs (n=8) despite the presence of IPSCs including large fIPSC components in nearby SPNs demonstrating that FSIs were not involved in the feed-forward inhibition of SPNs (Fig. 4b). The absence of excitation was not a slice preparation artifact because nEPSCs were readily elicited in all NPY-NGF neurons (Figs. 2 and 3).

A possible contribution by the sparse input to SPNs from NPY-PLTS neurons[19] was excluded using the same double transgenic optogenetic strategy employed when

Author Manuscript Author Manuscript Author Manuscript Author Manuscript

investigating the role of NPY-NGF interneurons (Supplementary Fig. 8). These results however did not rule out small depolarizing effects on FS and NPY-PLTS interneurons or that presynaptic facilitation of GABA release from these interneurons contributed to the inhibition of SPNs.

Finally, biophysical differences and stimulus intensity dependent dissociation of the feed-forward inhibition of SPNs and recurrent inhibition in ChAT interneurons[25] strongly suggest that these responses were not mediated by the same interneurons (Supplementary Fig. 7).

The pause-excitation population activity of ChAT interneurons regulates the activity of SPNs *in vitro* and *in vivo*

In behaving primates the most common reinforcement-related population activity of putative ChAT interneurons is a pause-excitation sequence[3,4,7-9]. Quantitative properties of the postsynaptic effects of this population response may not be evaluated adequately using ChR2 mediated synchronous activation alone because this approach does not reproduce the pause-associated reduction in cholinergic tone that may have significant effects via receptor deactivation[23,26] or recovery from desensitization [27] and because of the possibility of eliciting non-physiologically enhanced neurotransmitter release and abnormally high extracellular acetylcholine transients due to prolonged presynaptic depolarization and Ca^{++} influx. To overcome these problems we used optogenetic inhibition to elicit a pause excitation response by taking advantage of the fact that ChAT interneurons respond to brief hyperpolarization with semi-synchronous rebound firing[28]. ChAT interneurons expressing an enhanced variant of *Natronomonas Pharaonis* Halorhodopsin[29] (eNpHR3.0) exhibited normal intrinsic properties *in vitro* and responded to optical stimuli (green light, 200-300 ms) with hyperpolarizing responses and rebound action potentials (Fig. 5a, b). Cell attached and extracellular recordings showed that the majority of ChAT interneurons were spontaneously active and generated variable latency rebound firing following optical inhibition (Fig. 5b-e) that successfully approximated the pause-excitation population pattern of putative ChAT interneurons recorded *in vivo*[3,4,8,30] (Fig. 5c). The optically induced population activity of cholinergic interneurons elicited large amplitude GABAergic IPSPs in SPNs (Fig. 5c-e) that were secondary to the activation of Type-2 nicotinic receptors as shown by DHβE block (200 nM, n=5, Fig. 5e). The onset of the response followed the end of the light pulse with a short latency (∼50 ms), and was apparently initiated by the first cholinergic rebound spikes (Fig. 5c, d). The IPSP effectively blocked action potential generation in SPNs (Fig. 5c-e). A minority of the SPNs (n=5) exhibited an additional more delayed period of inhibition that was similarly blocked by DHβE (200 nM, n=2) and coincided with longer latency rebound activity of some ChAT interneurons (Fig. 5a, e). Current recordings revealed that the elicited synaptic response in SPNs resembled the compound response described above (Fig. 5d). These latter experiments were conducted using eNpHR1.0-mCherry (Methods) which is not expressed in axons and therefore circumvents any potential effects of direct axon terminal hyperpolarization[29,31].

Finally, we sought to confirm that the pause-excitation activity pattern of ChAT interneurons also exerts inhibitory control on projection neurons *in vivo*. We obtained single and multi-unit recordings in the dorsal striatum of freely moving mice expressing eNpHR3.0

Author Manuscript Author Manuscript Author Manuscript Author Manuscript

in ChAT interneurons with chronically implanted optrodes containing 4 movable tetrodes and a fixed, laser-coupled optic fiber. The optical stimulus was a 200 ms (n=9) or a 1000 ms (n=3) laser pulse (10-30 mW, 594 nm) delivered at fixed 20 s or 30 s intervals. None of the mice exhibited observable behavioral responses to the delivery of light pulses. Units were separated and classified as described in the Methods (Fig. 6a). The identity of ChAT interneurons was directly confirmed based on zero time lag optical inhibition.

Six isolated ChAT units were identified in four animals. These neurons exhibited irregular tonic activity that was similar to the firing pattern of putative ChAT interneurons described in primates as well as to optogenetically identified ChAT interneurons in the nucleus accumbens[32] (Fig. 6b). 200 ms optical inhibition elicited a pause excitation sequence characterized by nearly complete silencing during illumination followed by rebound firing (Fig. 6c). The rebound population activity lasted approximately 150 ms and exhibited a maximal firing rate of 370% of baseline that occurred about 45 ms after the offset of the stimulus and recovered exponentially with a time constant of 64 ms (Fig. 6c). The overall response and the characteristics of rebound excitation closely recapitulated the key properties of putative ChAT interneuron population responses recorded in a variety of behavioral paradigms[3,4,8,30].

The same optical stimuli elicited statistically significant inhibition of firing in putative SPNs including 7 isolated and 5 multiunit recordings of these neurons (Fig. 6d). The inhibition exhibited a rapid onset (112.5±90.8 ms delay from the end of the light to pulse to the first 50 ms PSTH bin below 2SD from the mean). Mean maximal inhibition was 84.7±15.3 % (defined as the mean firing rate *reduction* during the 2 most strongly inhibited consecutive bins) representing a significant change (p=0.0019, see Methods) for each putative SPN. (Note that the smaller magnitude of the maximal inhibition of the SPN population activity (74%, Fig. 6d) is due to averaging of multiple responses with different response latencies). The firing rate remained below a level of mean-2SD for 200±85.3 ms and recovered bi-exponentially from its minimal value with time constants of 190 ms (64% of peak) and 0.4 s (36% of peak, n=12). To confirm that the coincidence of the onset of the inhibition and the end of the light pulse reflected a causal relationship we also tested the effect of 1000 ms (n=3) light pulses. The inhibitory responses elicited by these stimuli were similarly timed to the end of the stimuli (Fig. 6d). Importantly, there was no indication of firing rate changes in the same units during either 200 or 1000 ms optical inhibition of ChAT interneurons (Fig. 6d).

Finally, inhibition resembling the responses of putative SPNs was also observed in 2 units that exhibited firing rates and waveforms different from putative SPNs (Fig. 6a) suggesting that some GABAergic interneurons may be regulated similarly to SPNs (Supplementary Fig. 9).

Discussion

This study demonstrates the existence of multiple GABAergic circuits that are activated by ChAT interneurons and examines their role in the regulation of the activity of SPNs. The detailed organization of these circuits remains incompletely understood. We show that NPY-

Author Manuscript Author Manuscript Author Manuscript Author Manuscript

NGF interneurons are directly activated by nicotinic synaptic input and elicit slow GABAeric inhibition in SPNs. The electrophysiological and circuitry properties of NPY-NGF interneurons appear well suited for transmitting cholinergic population responses. Specifically, the slow time course of the nEPSP is expected to facilitate integration of synaptic inputs during semi-synchronous activation of ChAT interneurons while the high current threshold and the feed-forward inhibition of NPY-NGF interneurons may prevent their spurious activation by randomly coincident presynaptic inputs. Further, the utilization of $GABA_A$-slow, which, based on experiments using low affinity antagonists[15], subtype specific modulators[12,14,15,33], diffusional interference[15] and blockade of GABA transport[14-16] appears to involve volume transmission and possibly the activation of extrasynaptic receptors[33,34] enables high fidelity, widespread inhibition of large neuron populations by single presynaptic elements. These characteristics, together with the extremely high probability of connectivity and electrotonic coupling of NPY-NGF neurons support uniform inhibition of SPNs despite the relatively small population size of these interneurons[18].

Biophysical and pharmacological evidence also demonstrated the cholinergic activation of a second, separate GABAergic input to SPNs responsible for the fIPSC. The possibility that the fIPSC is generated by direct synaptic contacts of NPY-NGF neurons onto SPNs while the sIPSC originates through volume transmission of GABA released from a larger set of terminals of the same interneurons is inconsistent with the observation that in a large number of paired recordings of NPY-NGF interneurons and SPNs (n=40, 11 this study and 29 in our earlier report[18]) no fast IPSC components have been observed. Presynaptic nicotinic facilitation or GABA release could mediate the fIPSC[35-37], possibly involving terminals of FS interneurons that express nicotinic receptors, but a presynaptic mechanism is inconsistent with the absence of an asynchronous barrage of mini-IPSCs during the compound response[35,36]. However, presynaptic facilitation of GABA release from synapses responsible for the sIPSC cannot be excluded and this mechanism could account for the IPSCs elicited in SPNs by single ChAT interneurons. Thus, the simplest hypothesis regarding the origin of the fIPSC is that it is elicited by action potential firing in a type of GABAergic interneuron that is distinct from NPY-NGF, NPY-PLTS and FS neurons. The most likely candidates are calretinin[38] (CR) and tyrosine hydroxylase (TH) expressing interneurons[39]. Similarly, the recurrent inhibition of ChAT interneurons is also likely to originate from a subset of CR or TH interneurons that appear to be distinct from those mediating the fIPSC. ChAT interneurons form a complex network with their GABAergic postsynaptic partners that includes 2 different inhibitory feedback mechanisms, electrical coupling between NPY-NGF neurons and inhibition among some of the GABAergic interneurons themselves. This network may be important for shaping and processing the transient population responses of ChAT interneurons and may contribute to the generation and behaviorally contingent frequency transitions of gamma range oscillations in the neostriatum[40].

We also investigated the effect of a physiologically realistic pause-excitation activity pattern of ChAT interneurons on the spontaneous firing of putative SPNs in freely moving mice. SPNs exhibited a rapidly developing, powerful inhibitory response that coincided with the

Author Manuscript Author Manuscript Author Manuscript Author Manuscript

synchronous firing of ChAT interneurons confirming our *in vitro* results. Interestingly, brief (<1 s) silencing of ChAT interneurons did not elicit an observable effect suggesting the absence of tonic muscarinic modulation of SPNs or their synaptic inputs[23,26] or sustained nicotinic receptor driven GABAergic inhibition. Therefore the pause response of ChAT interneurons may not affect striatal function primarily through the regulation of the firing of SPNs but by involving other mechanisms, including reversal of the permissive nicotinic facilitation of dopamine release[41,42]. A potential involvement of more complex muscarinic effects[26] cannot be ruled out based on our experiments. In addition, the *in vivo* and *in vitro* responses of SPNs to manipulation of ChAT interneuron activity appear to differ in the dorsal striatum from those in the nucleus accumbens[32] suggesting significant differences in the circuit organization of the 2 brain areas.

From a behavioral perspective, feed-forward inhibition of SPNs by ChAT interneurons may contribute to the interruption and reorientation of ongoing behavior when salient stimuli are encountered. Synchronous activation of ChAT interneurons by intralaminar thalamic inputs that carry information about alerting stimuli[43] is expected to trigger feed-forward inhibition of SPNs and interrupt the ongoing activity of cortico-basal ganglia loops. Furthermore, feed-forward inhibition may aid adaptive reorientation of behavior by promoting preferential activation of specific SPNs and cortico-basal ganglia circuits that are responsive to the thalamo-striatal excitatory inputs activated by the alerting stimuli. The targeting of SPNs by the same excitatory thalamic input responsible for synchronous cholinergic activation may also explain why inhibition of the firing of SPNs is less consistently observed during naturally occurring than optogenetically elicited synchronous activity of ChAT interneurons in behaving animals[44]. Importantly, since ChAT interneurons respond primarily to stimuli with conditioned reinforcement value the feed-forward inhibitory circuit can selectively gate the impact of external stimuli on ongoing behavior depending on the behavioral significance of these stimuli.

Finally, the inhibitory circuits described here may causally link the partial loss of ChAT interneurons[45] and the motor symptoms of Tourette syndrome as previously hypothesized [46].

Methods

1. Transgenic mice

Cholinergic interneurons were targeted in homozygotic *ChAT-IRES-Cre* transgenic mice (*B6;129S6-Chat<tme^{1}(cre)Lowl>/J*, Jackson Laboratory). The role of NPY interneurons was examined in double transgenic mice generated by cross breeding the *ChAT-IRES-Cre* strain with a *B6.FVB-Tg(NPY-hrGFP)^{1}Lowl/J* strain of mice (Jackson Laboratory). GFP targeted paired recording from ChAT interneurons and SPNs was performed using *B6.Cg-Tg(RP23-268L19-EGFP)$_{2}$Mik/J* mice (Jackson Laboratory).

2. Production of AAV-2, AAV-5 and integration deficient lentivirus vectors

Adeno-associated virus serotype 2 (AAV-2) was used for the expression of ChR2-YFP and serotype 5 (AAV-5) virus for eNpHR3.0-YFP and ChR2-mCherry. The AAV-2 vector was

Author Manuscript Author Manuscript Author Manuscript Author Manuscript

produced at Vector Biolabs (Philadelphia, PA) using transfer vector DNA designed and constructed by K.D. The AAV-5 vectors were produced by the vector core of the University of North Carolina for K.D. The transfer vector plasmids and the transgene constructs were designed by K.D. (http://www.stanford.edu/group/dlab/optogenetics/sequence_info.html).

Lentivirus mediated, Cre/lox controlled expression of eNpHR1.0-mCherry was carried out with integration deficient lentiviral (IDL) particles to prevent chromosomal rearrangements that may occur across multiple proviral loxP or lox2227 recombination sites when integrating virus is employed. IDL particles were produced in 293FT cells (Invitrogen) grown to 95-100% confluence in DMEM (+10% FBS and 1% L-glutamine) using TransIT-293 (Mirus) transfection agent as described previously[47]. Briefly, confluent 293FT cells in each of 6, 175 cm^2 flasks (Falcon) were co-transfected with 22 μg of the lentiviral transfer vector DNA (*pLenti:EF1:DOI:eNpHR1.0-mCherry:WPRE*) and the second generation packaging plasmids *pCMV-dR8.74-D64V* (15 μg), and *pMD2.G* 5 μg; (Addgene, 12259) supplemented with a plasmid carrying a suppressor of a dsRNA inhibitor (*pAdvantage*, Promega, 2 μg). The *pCMV-dR8.74-D64V* plasmid encodes the lentiviral integrase carrying a D64V point mutation that completely blocks proviral integration[48] and was a gift from Dr. Rafael Yanez-Munoz. 24 hours after transfection the medium was changed to a viral production medium (Ultraculture, Lonza, + 1% pen-strep, 1% Na-Pyruvate, and 5 mM Na-Butyrate) and 48 hours post-transfection the virus-containing supernatant was collected and concentrated with ultracentrifugation. The titer of the concentrated IDL was not directly determined, but comparison with lentivirus stocks of known titer injected in mouse brains indicated that it approached 10^9 IU/ml.

The eNpHR1.0-mCherry transgene was produced by adding the ER export and membrane localization signals described by Gradinaru et al.,[31] in 2 rounds of extension PCR using a high fidelity DNA polymerase (Accuprime *Pfx*, Invitrogen) to the coding sequence of NpHR-mCherry produced by K.D. (http://www.stanford.edu/group/dlab/optogenetics/sequence_info.html). The primer sequences for the first and second PCR rounds were, respectively: *5′,-GTCGTCTCTCTGTTCTCTCTGCTTCAGGACACAGAGACCCTGCCTCCCGTGACCGAGAGT-3′* and *5′-TTACACCTCGTTCTCGTAGCAGAACTTGTACAGCTCGTCCATGC-3′*, and *5′-GGCCTGCGCTAGCGCCACCATGAGGGGTACGCCCCTGCTCCTCGTCGTCTCTCTGTTCTCTCTGCTTCAG-3′*, and *5-′CggacccatatgGGCGCGCCTTACACCTCGTTCTCGT-3′*. The PCR product was subcloned in an inverted orientation between the loxP/lox2722 flanking recombination sites replacing the ChR2-YFP coding sequence in an *AAV:EF1:DOI:ChR2-YFP:WPRE* plasmid produced and provided by K.D., from which subsequently the entire expression cassette (*EF1:DOI:eNpHR1.0-mCherry:WPRE*) was cloned into a 3rd-generation (Tat-independent) self-inactivating lentiviral expression vector. Detailed map is available from T.K. on request.

3. Intracerebral virus injection

All in vivo and in vitro surgical procedures were performed in accordance with the National Institutes of Health Guide to the Care and Use of Laboratory Animals and with the approval

Author Manuscript Author Manuscript Author Manuscript Author Manuscript

of the Rutgers University Institutional Animal Care and Use Committee. The virus injection surgeries were performed in a custom built surgical setup inside a isolation cabinet under Biosafety Level-2 (BL-2) confinement. Mice were anesthetized with isoflurane and the skull was exposed under antiseptic conditions using local anesthesia with bupivacaine. A small burr hole was drilled at coordinates 0.5 -1.0 mm anterior to Bregma, 1.5-2.2 mm lateral. 0.5-1.5 μl of concentrated virus stock solution was injected using a Nanoject-2 pressure injection apparatus using glass pipettes over 10-40 minutes at a depth of 2.4-2.7 mm from the surface of the brain. Animals were housed in a BL-2 safety cabinet for at least 6 days. Experiments were conducted 7-30 days following injection.

4. Immunocytochemistry

Fixation was performed after establishing anesthesia with ketamine (400 mg/kg, i.p.) with transcardial perfusion using 10 ml of ice cold oxygenated Ringer solution followed by 75-100 ml of 4% paraformaldehyde and 15% saturated picric acid in 0.15 M phosphate buffer. Brains were kept in the same fixative overnight. 60 μm sections were cut on a Vibratome. The immunocytochemical labeling of ChAT included pre-incubation in 10% methanol and 3% hydrogen peroxide in phosphate buffered saline (PBS), blocking of nonspecific binding with 10% normal donkey serum, 3% bovine serum albumin in a 0.5% Triton X-100 solution in PBS, followed by incubation in the blocking solution containing 1:200 goat anti-ChAT primary antibody (cat. # AB144P; Millipore Corp.) for 48 hours at room temperature. After wash, sections were incubated in 1:100 donkey anti-goat IgG conjugated with Alexa-594 in PBS at room temperature overnight. Sections were mounted in Vectashield medium.

5. *In vitro* optical stimulation

ChR2-YFP was activated using a 750 mW blue LED (www.Cree.com) with light projected onto the slice through the condenser of the microscope with the bottom DIC polarizer removed. The intensity and duration of the illumination were controlled through a D/A converter output of a ITC-18 digitizer and a Mightex SLA LED driver. eNpHR3.0-YFP and eNpHR1.0-mCehrry were activated with alternating pulses of 200-300 ms green (514±20 nm) and blue (470±20 nm) light delivered through the epifluorescence illumination pathway using Chroma Technologies filter cubes under temporal control with a Uniblitz shutter (Vincent Associates, Rochester NY, USA). Blue light was delivered to facilitate recovery from photodesensitization. Optical stimuli were delivered at 30-60 s intervals to allow recovery to baseline.

6. *In vivo* optical stimulation

125 μm multi mode optic fibers (Part #AFS105/125Y; Thor Labs, Newton NJ, USA) were chronically implanted as part of the optrode described in *#8*. To minimize tissue damage and increase the lateral distribution of light, optical fibers were etched by immersing ∼200 μm of the tip of the fiber in hydrofluoric acid (Sigma-Aldrich) overlaid with mineral oil and then slowly lifting the fiber tip into the protective oil layer (over ∼ 30-60 min) resulting in a smooth, gradual taper and a tip diameter of <50 μm. Implanted fibers were coupled to a 594 nm DPSS laser (LaserGlow Technologies, Toronto Canada) via modified LC connectors

Author Manuscript Author Manuscript Author Manuscript Author Manuscript

(Part # 86024-5500; Thor Labs, Newton NJ, USA) and ceramic attachments encasing the external end of the fiber. Light intensity at the fiber tip was measured before implantation as 10-30 mW. Illumination duration was controlled via a TTL-gated shutter with a transition time of less than 0.5 ms (Uniblitz LS2; Vincent Associates, Rochester NY, USA). Stimulation timing was controlled via Spike2 software running a CED micro MKII Digitizer (Software and hardware from Cambridge Electronic Design, Cambridge, England).

7. *In vitro* slice preparation and recording

Transgenic mice were 60-390 days old when sacrificed. Brain slices were prepared and visualized whole cell recordings performed as described in detail in ref:[10] Voltage clamp recordings were performed with a CsCl based medium in some cases including QX-314 (5-15 mM). Action potentials were elicited in ChAT interneurons usually in voltage clamp with 3-5 ms, 70-100 mV pulses. These recordings used KCl based internal solution with $E[Cl^-]\sim$-10 mV to facilitate detection of recurrent IPSCs. Most neurons were intracellularly labeled with Alexa-594 or Alexa-488 (25-75 μM).

8. Chronic *in vivo* extracellular recording

Optrodes were composed of four independently movable tetrodes mounted in a 5-cannula array surrounding a central optic fiber with lateral distances between the 5 elements set at 200 μm. Tetrode wires were gold-plated to impedances of <400 kOhm measured at 1 kHz, no more than 1 hour before implantation. Coordinates targeting dorsal striatum were, anterior, +0.5-1.0 mm, lateral, 1.6-2.0 mm and ventral, -2.4-2.7 mm (relative to Bregma). Animals were implanted with optrodes > 7 days post virus injection.

Wires were advanced slowly until units were encountered. The recorded extracellular potential was pre-amplified 20× using a headstage pre-amplifier (Plexon, Dallas Texas, USA) and further amplified 100× and band-pass filtered (0.1-10,000 Hz) using an analog amplifier (Grass Technologies, West Warwick Rhode Island, USA), digitized at 25 kHz (micro MKII Digitizer, Cambridge Electronic Design, Cambridge, England) and recorded for off-line analysis using Spike2 software (Cambridge Electronic Design, Cambridge, England).

9. Analysis of *in vitro* data

Analysis was performed in Axograph2.0 (J. Clements) or routines written in IgorPro (WaveMetrics, Oswego, CA). Rise times were defined as the time difference between the data points at which the amplitude of the response was 10 and 90 % of peak, respectively. For the analysis of the correlation of fIPSC and sIPSC amplitudes individual response amplitudes were defined as the mean within a 1 ms (fIPSC) or 15-35 ms (sIPSC) window (Fig. 1f). The wide window averaging was carried out to eliminate the contribution of the uncorrelated stochastic channel noise associated with the sIPSC. An exponential function was then fitted to the fIPSC and sIPSC amplitudes of subsequent compound responses expressed as functions of recording time, which revealed that both amplitudes decayed over repeated stimulations. The exponentially fitted trend of amplitude decay was then subtracted from the individual amplitudes and the de-trended amplitudes were expressed relative to the respective average fIPSCs and sIPSCs amplitudes, thus defining ΔfIPSC and ΔsIPSC (Fig.

Author Manuscript Author Manuscript Author Manuscript Author Manuscript

1f). This procedure does remove a source of correlated variance of unknown origin but the uncorrelated nature of the residual variance excludes in itself the possibility of shared receptor mechanisms or neurotransmitter pools underlying the 2 response components.

10. Analysis of *in vivo* data

Spike2 software was used for spike detection and sorting. Signals were band-pass filtered (300-6,000 Hz, digital 2-pole Butterworth filter) and an appropriate spike trigger threshold was set by the experimenter (approximately 3-5 times the SD of the noise). Wavemarks defined as 0.5 ms pre and 1.0 ms post peak threshold crossing were extracted from each channel when at least one channel was triggered. After detection, the mean of the peak amplitudes (negative going) on the four channels was measured and this data was combined with the relative ratios of the peaks on the four channels yielding 5 variables from which 3 principal components were extracted using a PCA routing of Spike2. The events were then projected in thus defined 3D space and were automatically over-clustered using the K-mean statistics (10-20 clusters are initially cut for data actually having less than 5 units). Clusters manually classified as noise on the basis of waveform shapes and inter-stimulus interval (ISI) histograms were discarded. The remaining potential units were then recombined and reclassified the same way a second time, with the effect of reducing the bias introduced in the first iteration by the noise and improving the extraction of principal components most discriminative among extracellular spikes. The identified clusters were then subjected to PCA analysis based on multidimensional data defined by all amplitudes values in the spike waveforms. K-means were again used to automatically over-cluster the data, and the clustering information from waveforms and relative amplitude ratios was reconciled manually. Auto and cross-correlation histograms were constructed and units were classified as putative single units if there was a clear refractory period (>3 ms) and if in the ISI histogram 10% or less of the spikes in the first 50 ms occurred in the first 5 ms[49]. Unit clusters that had classifiable waveforms similar to single units but did not meet these criteria were classified as multiple unit recordings.

Differences in waveform shape and firing pattern as well as optical responses were used to classify cell types. In accordance with previous reports[58,63,64], putative SPN single units had firing rates <2 Hz (mean=0.74 Hz, SD=0.62) and band pass filtered (300-6,000 Hz) waveform valley widths >0.35 ms (mean=0.51 ms, SD=0.09)[50]. ChAT units were identified based on zero latency optical inhibition. Surprisingly, the waveforms of ChAT and SPN units were similar, the most reliable difference being an initial positive phase present only in ChAT units (Fig. 6). Spikes of ChAT units fired tonically whereas SPNs tended to fire single spikes or bursts interspersed with long (>1s) periods of silence. Units classified as “other neurons” had firing rates similar to ChAT interneurons but had significantly shorter waveforms than all other unit classes and their firing rate was not directly modulated by illumination.

To examine the relationship between optical stimulation and changes in the firing rate of SPNs, PSTHs were constructed using 50 ms binning and the mean and the SD of the spike number per bin were calculated for the 10-20 s preceding the stimulus (20-40 bins). A

Author Manuscript Author Manuscript Author Manuscript Author Manuscript

statistically significant change in firing rate change was defined as 2 consecutive bins outside mean±2SD defining a significance level of p=0.0019.

11. Statistical methods

Due to the small number of observations in most cases the nonparametric Wilcoxon rank-sum test was used to compare means of populations. These calculations and linear regression analysis were performed in IgorPro or StatView. Population measurements are reported as mean ± An exponential function standard deviation unless otherwise indicated. The statistical significance of firing rate changes *in vivo* were determined as described above (#10).

Supplementary Material

Refer to Web version on PubMed Central for supplementary material.

Acknowledgments

We thank Dr. J. Berlin for confocal microscopy, Dr. L. Zaborszky for providing ChAT-EGFP mice, Dr. R. Yanez-Munoz for providing integration deficient *pCMV-dR8.74-D64V* plasmid DNA and for advice regarding virus production, Dr. N. Altan-Bonnet, Dr. W. Friedman and Dr. Haesun Kim for generously providing access to an ultracentrifuge facility and other equipment in their laboratories, C.T. Unal and Dr. A. Kreitzer for valuable discussion, Dr. A. Berenyi, Dr. S. Fujisawa, and Dr. M. Vandecasteele, for advise regarding *in vivo* recording methods, H. Xenias for help with confocal imaging, F. Shah for help with immunocytochemical procedures and other technical assistance and I. Tadros for virus injections. The research was supported by NS072950 and a Busch Biomedical Research Grant of Rutgers University to T.K., and NS034865 to J.M.T. and Rutgers University funds.

References

1. Graybiel AM. Neurobiol Learn Mem. 1998; 70:119–36. [PubMed: 9753592]
2. Schultz W. J Neurophysiol. 1998; 80:1–27. [PubMed: 9658025]
3. Morris G, Arkadir D, Nevet A, Vaadia E, Bergman H. Neuron. 2004; 43:133–43. [PubMed: 15233923]
4. Joshua M, Adler A, Mitelman R, Vaadia E, Bergman H. J Neurosci. 2008; 28:11673–84. [PubMed: 18987203]
5. Hyland BI, Reynolds JN, Hay J, Perk CG, Miller R. Neuroscience. 2002; 114:475–92. [PubMed: 12204216]
6. Kimura M, Rajkowski J, Evarts E. Proc Natl Acad Sci U S A. 1984; 81:4998–5001. [PubMed: 6589643]
7. Apicella P. Trends Neurosci. 2007; 30:299–306. [PubMed: 17420057]
8. Aosaki T, et al. J Neurosci. 1994; 14:3969–84. [PubMed: 8207500]
9. Aosaki T, Kimura M, Graybiel AM. J Neurophysiol. 1995; 73:1234–52. [PubMed: 7608768]
10. Tecuapetla F, Koos T, Tepper JM, Kabbani N, Yeckel MF. J Neurosci. 2009; 29:8977–90. [PubMed: 19605635]
11. Pearce RA. Neuron. 1993; 10:189–200. [PubMed: 8382497]
12. Banks MI, Li TB, Pearce RA. J Neurosci. 1998; 18:1305–17. [PubMed: 9454840]
13. Tamas G, Lorincz A, Simon A, Szabadics J. Science. 2003; 299:1902–5. [PubMed: 12649485]
14. Karayannis T, et al. J Neurosci. 2010; 30:9898–909. [PubMed: 20660272]
15. Szabadics J, Tamas G, Soltesz I. Proc Natl Acad Sci U S A. 2007; 104:14831–6. [PubMed: 17785408]
16. Banks MI, White JA, Pearce RA. Neuron. 2000; 25:449–57. [PubMed: 10719898]
17. Overstreet LS, Jones MV, Westbrook GL. J Neurosci. 2000; 20:7914–21. [PubMed: 11050111]

Author Manuscript Author Manuscript Author Manuscript Author Manuscript

18. Ibanez-Sandoval O, Tecuapetla F, Unal B, Shah F, Koos T, Tepper JM. Journal of Neuroscience. 2011
19. Gittis AH, Nelson AB, Thwin MT, Palop JJ, Kreitzer AC. J Neurosci. 2010; 30:2223–34. [PubMed: 20147549]
20. Capogna M, Pearce RA. Trends Neurosci. 2011; 34:101–12. [PubMed: 21145601]
21. Hill JA Jr, Zoli M, Bourgeois JP, Changeux JP. J Neurosci. 1993; 13:1551–68. [PubMed: 8463835]
22. Koos T, Tepper JM. Nat Neurosci. 1999; 2:467–72. [PubMed: 10321252]
23. Koos T, Tepper JM. J Neurosci. 2002; 22:529–35. [PubMed: 11784799]
24. Chang HT, Kita H. Brain Res. 1992; 574:307–11. [PubMed: 1638402]
25. Sullivan MA, Chen H, Morikawa H. J Neurosci. 2008; 28:8682–90. [PubMed: 18753369]
26. Ding JB, Guzman JN, Peterson JD, Goldberg JA, Surmeier DJ. Neuron. 2010; 67:294–307. [PubMed: 20670836]
27. Giniatullin R, Nistri A, Yakel JL. Trends Neurosci. 2005; 28:371–8. [PubMed: 15979501]
28. Wilson CJ. Neuron. 2005; 45:575–85. [PubMed: 15721243]
29. Gradinaru V, et al. Cell. 2010; 141:154–65. [PubMed: 20303157]
30. Apicella P, Ravel S, Sardo P, Legallet E. J Neurophysiol. 1998; 80:3341–4. [PubMed: 9862929]
31. Gradinaru V, Thompson KR, Deisseroth K. Brain Cell Biol. 2008; 36:129–39. [PubMed: 18677566]
32. Witten IB, et al. Science. 2010; 330:1677–81. [PubMed: 21164015]
33. Olah S, et al. Nature. 2009; 461:1278–81. [PubMed: 19865171]
34. Banks MI, Pearce RA. J Neurosci. 2000; 20:937–48. [PubMed: 10648698]
35. Wonnacott S. Trends Neurosci. 1997; 20:92–8. [PubMed: 9023878]
36. McGehee DS, Heath MJ, Gelber S, Devay P, Role LW. Science. 1995; 269:1692–6. [PubMed: 7569895]
37. De Rover M, Lodder JC, Schoffelmeer AN, Brussaard AB. Synapse. 2005; 55:17–25. [PubMed: 15499607]
38. Kubota Y, Mikawa S, Kawaguchi Y. Neuroreport. 1993; 5:205–8. [PubMed: 7507722]
39. Ibanez-Sandoval O, et al. J Neurosci. 2010; 30:6999–7016. [PubMed: 20484642]
40. Berke JD. Eur J Neurosci. 2009; 30:848–59. [PubMed: 19659455]
41. Zhou FM, Liang Y, Dani JA. Nat Neurosci. 2001; 4:1224–9. [PubMed: 11713470]
42. Rice ME, Cragg SJ. Nat Neurosci. 2004; 7:583–4. [PubMed: 15146188]
43. Matsumoto N, Minamimoto T, Graybiel AM, Kimura M. J Neurophysiol. 2001; 85:960–76. [PubMed: 11160526]
44. Hikosaka O, Sakamoto M, Usui S. J Neurophysiol. 1989; 61:814–32. [PubMed: 2723722]
45. Kataoka Y, et al. J Comp Neurol. 2010; 518:277–91. [PubMed: 19941350]
46. Leckman JF, Vaccarino FM, Kalanithi PS, Rothenberger A. J Child Psychol Psychiatry. 2006; 47:537–50. [PubMed: 16712630]
47. Han X, et al. Neuron. 2009; 62:191–8. [PubMed: 19409264]
48. Yanez-Munoz RJ, et al. Nat Med. 2006; 12:348–53. [PubMed: 16491086]
49. Jog MS, et al. J Neurosci Methods. 2002; 117:141–52. [PubMed: 12100979]
50. Berke JD. J Neurosci. 2008; 28:10075–80. [PubMed: 18829965]

Author Manuscript Author Manuscript Author Manuscript Author Manuscript

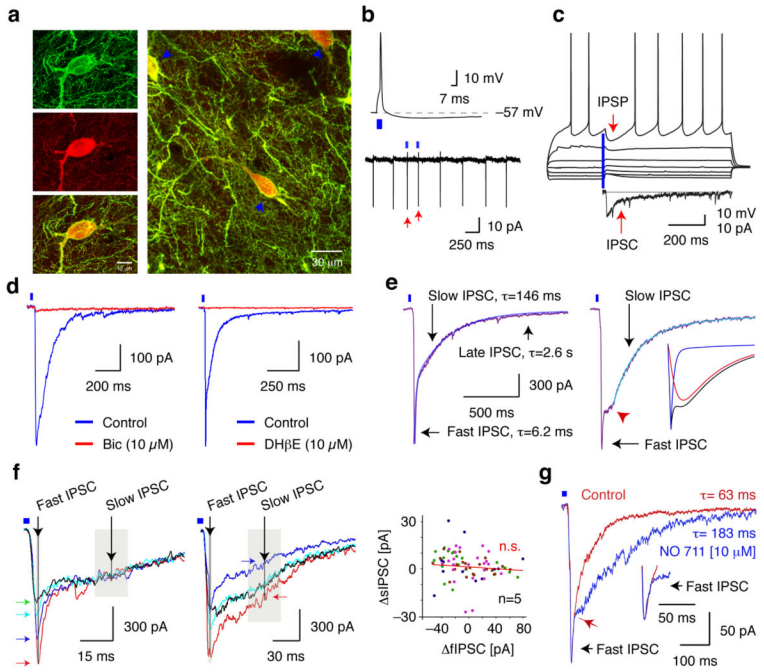

Figure 1. Characterization of GABAergic IPSCs elicited in SPNs with optogenetic stimulation of ChAT interneurons

a. Confocal images of a ChR2-YFP expressing neuron (top left) immunostained for ChAT (middle; bottom: overlay). A larger field is shown at the right.

b. *Top:* Optically elicited action potential in a ChAT interneuron. *Bottom:* A cell-attached recording of spontaneous activity and optically evoked action potentials (red arrows) of a ChAT interneuron.

c. Optogenetically elicited IPSPs in an SPN (arrow) efficiently blocked firing induced by current injection. Bottom trace, corresponding IPSC, (V_{hold}=-80 mV).

d. Optogenetically elicited IPSCs in 2 SPNs (blue traces) were blocked by bicuculline (left) or DHβE (right, red traces).

e. Kinetic components of the compound IPSC. *Left:* 3 distinct components of the IPSC exhibiting different τ_{decay} values. *Right:* Non-monotonic transition between the fIPSC and the sIPSC. Note the negative inflection following the transition (red arrowhead). *Inset:* Decomposition of the compound IPSC (black trace) into a fIPSC (blue trace) and a sIPSC (red trace).

f. Independent trial-to-trial amplitude variance of the fIPSC and the sIPSC. *Left*: overlay of 4 responses exhibiting identical sIPSC but different fIPSC components (colored arrows point to fIPSC peaks). Shaded areas are averaging windows. *Middle:* variable sIPSC components. *Right:* relative sIPSC amplitudes plotted against corresponding relative peak fIPSC amplitudes (n=5). Red line is linear regression (p>0.2).

g. Inhibition of GAT-1 selectively prolongs the sIPSC. Note that the fIPSC is unaffected (arrow and inset). Red arrow, transition point of the response components. In all figures blue bars represent optical stimuli.

Author Manuscript Author Manuscript Author Manuscript Author Manuscript

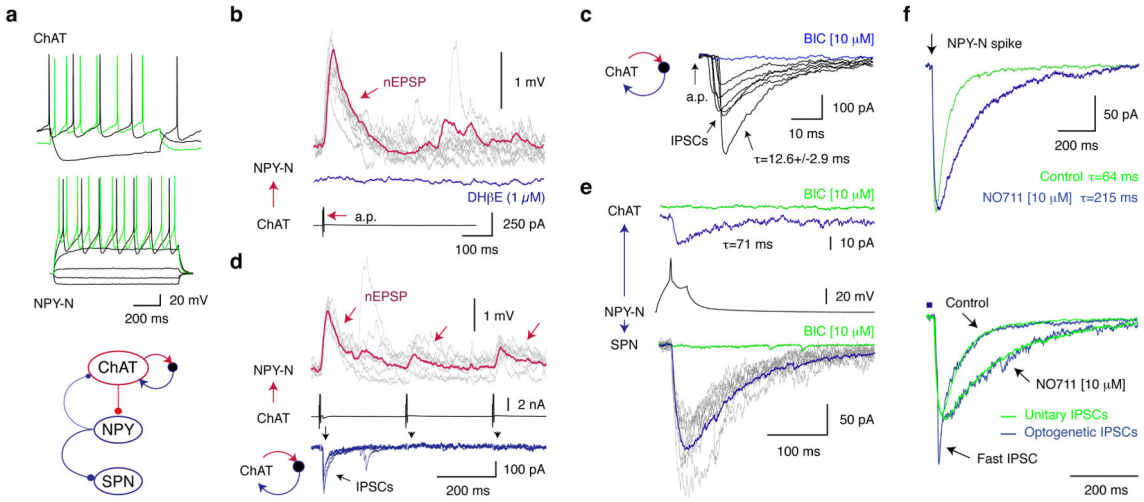

Figure 2. Synaptic interactions of ChAT and NPY-NGF interneurons and SPNs

a. *Top:* Characteristic passive and active properties of ChAT and NPY-NGF interneurons. *Bottom:* Synaptic circuitry of a ChAT and a NPY-NGF interneuron and a SPN recorded simultaneously (same as in *a, c-f*). GABAergic (blue) and nicotinic (red) interactions are indicated. Circular arrow represents recurrent inhibition.

b. Action potentials of the ChAT interneuron elicited in voltage clamp (bottom) elicited nEPSPs in the NPY-NGF interneuron (top; red, average) that were blocked by DHβE (blue).

c. Recurrent GABAergic IPSCs in the same ChAT interneuron (spike subtracted). Note the short τ_{decay} of the IPSC and block by bicuculline (blue trace).

d. Train stimulation of the ChAT interneuron (middle) elicits nEPSPs in the NPY-NGF neuron (top traces, arrows). Note partial depression of the nEPSPs contrasted with the complete failure of the recurrent IPSC after the first stimulus (bottom traces, arrowheads).

e. Spiking in the NPY-NGF interneuron (middle) elicits IPSCs in the SPN (bottom; blue, average) and the ChAT interneuron (top, blue, average). Note the slow time course of the IPSCs and the absence of a fIPSC in the SPN. Bicuculline block, green.

f. *Top:* Inhibition of GAT-1 increases τ_{decay} of the IPSC elicited in an SPN by an NPY-NGF interneuron (different neurons than in *e-f*). *Bottom*: Overlay of the same IPSCs (green traces) with optogenetic IPSCs recorded under the same pharmacological conditions (blue, same as in Fig. 1). Unitary responses were scaled in amplitude. Note the similarity of rise times and τ_{decay}.

Author Manuscript Author Manuscript Author Manuscript Author Manuscript

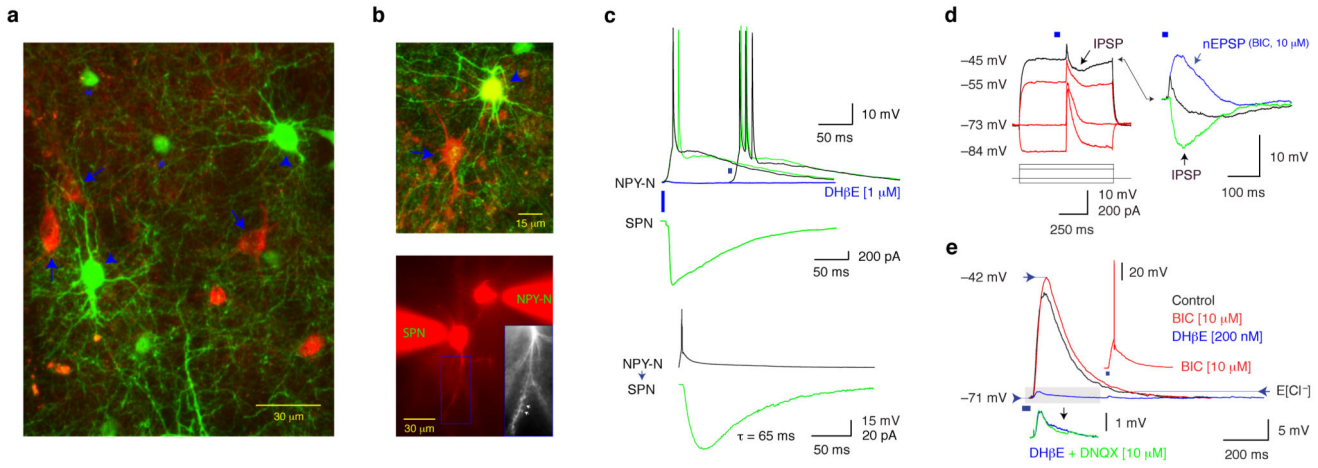

Figure 3. Optogenetic activation of ChAT interneurons elicits nEPSPs and GABAergic IPSPs and triggers action potential firing in NPY-NGF interneurons

a. Confocal image of ChAT interneurons expressing ChR2-mCherry (arrows) and 2 EGFP expressing NPY-NGF neurons (arrowheads) in a ChAT-Cre/NPY-GFP mouse.

b. *Top:* Confocal images of a NPY-NGF interneuron (arrowhead) and a simultaneously recorded nearby SPN intracellularly labeled with Alexa 594 (arrow). *Bottom:* Photomicrographs of the neurons during recording. *Inset:* high magnification showing SPN dendritic spines (arrows, same neurons as in *d-e*).

c. *Top panel*: Optical stimulation of ChAT interneurons elicited large amplitude depolarizations and action potentials in a NPY-NGF interneuron that were blocked by DHβE (blue trace). Simultaneously elicited optogenetic compound IPSC in the SPN (bottom green trace). *Bottom panel:* Single action potential in the NPY-NGF neuron (black trace) elicited a slow IPSC in the SPN (green trace).

d. EPSP-IPSC sequence elicited with optical stimulation of ChAT interneurons in an NPY-NGF neuron (different neurons from *b-e*). *Left*: reversal of the IPSP (arrow). *Right*: The IPSP (green trace), the compound response (black trace) and the isolated nEPSP (blue trace) recorded at ∼-45 mV. Note the large amplitude and slow time course of the isolated IPSP.

e. The compound response of another NPY-NGF interneuron (black trace) was gradually increased in amplitude by application of bicuculline (red trace), leading to action potential firing (top inset). The isolated nEPSP (red trace) was blocked by ∼95% by 200 nM DHβE (blue trace). The residual response (blue trace, bottom inset) was not DNQX sensitive (green trace).

Author Manuscript Author Manuscript Author Manuscript Author Manuscript

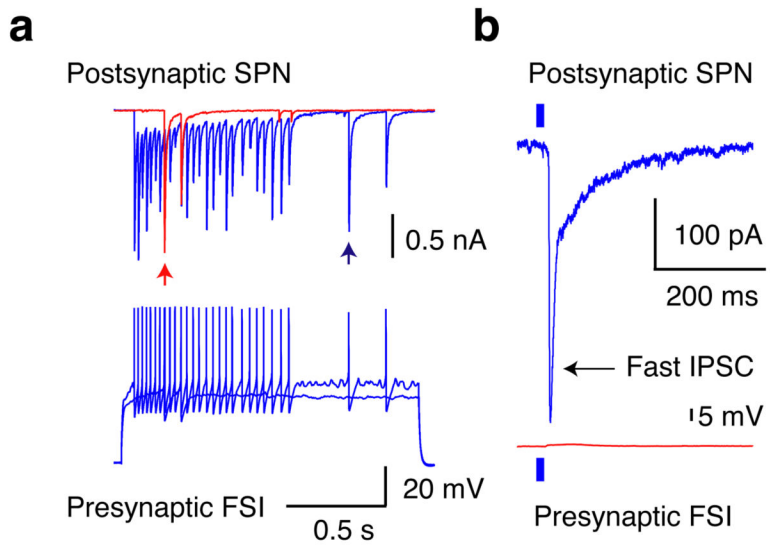

Figure 4. FSIs do not mediate the inhibition of SPNs by ChAT interneurons

a. Paired recording from a synaptically connected FSI and SPN. Intracellularly injected current pulses in the interneuron elicit voltage responses that identify it as an FSI (bottom). Note the typical large amplitude IPSCs elicited in the SPN (arrows).

b. Optical stimulus (blue bar) elicits a compound IPSC, including a large fIPSC in the SPN (blue trace, top) but fails to trigger action potentials or large depolarizing potentials in the FS interneuron (red trace, bottom). Compare to the responses elicited in NPY-NGF neurons in Fig. 3d, g.

Author Manuscript Author Manuscript Author Manuscript Author Manuscript

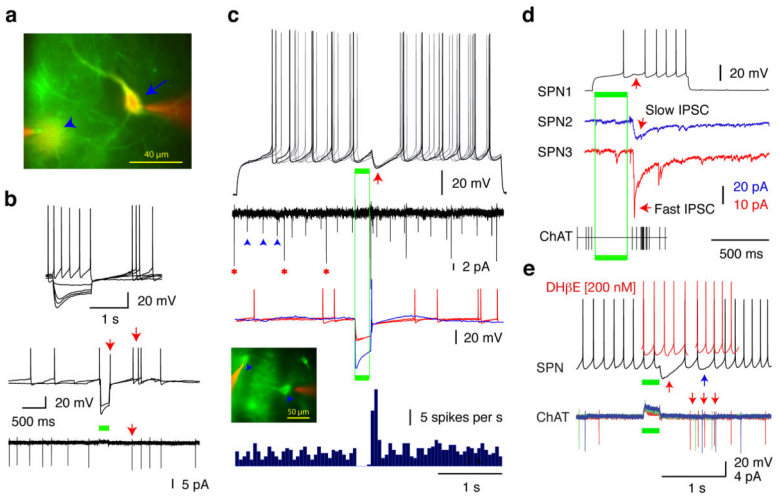

Figure 5. Optogenetically reproduced pause-excitation population response of ChAT interneurons elicits powerful inhibition in SPNs *in vitro*

a. Photomicrograph of eNpHR3.0-YFP-expressing ChAT interneurons (arrow, arrowhead) labeled intracellularly with Alexa 594 (red).

b. *Top*: Responses of an eNpHR3.0-YFP expressing ChAT interneuron to intracellular current (*a*, arrow). Whole cell (middle) and cell-attached (bottom) recordings demonstrated spontaneous activity and large amplitude optogenetic hyperpolarization (green bar) leading to rebound excitation (arrows).

c. Synaptic responses of a SPN to a pause-excitation population response of ChAT interneurons. *Top:* Rebound excitation of the interneurons triggered coincident large IPSPs (arrow) that efficiently blocked action potential generation. *Middle*: Spike trains of ChAT interneurons recorded using cell-attached (asterisks) and extracellular (arrowheads) recording (second trace from top) and in current clamp (color traces). *Inset*: eNpHR3.0-YFP expressing ChAT interneurons and cell attached recording pipettes (red). *Bottom*: PSTH of ChAT interneurons demonstrating pronounced pause-excitation activity.

d. Simultaneous current recordings (blue and red) from 2 SPNs showing IPSCs elicited by the rebound activation of ChAT interneurons (bottom) induced using eNpHR1.0-mCherry. Simultaneous voltage recording from a third SPN showed optically elicited spike delay (top, arrow). *Bottom*: Extracellular recording of a ChAT interneuron (spikes, vertical lines) showed optical inhibition and rebound firing.

e. *Top*: Short and long latency inhibition (black trace, red and blue arrows) in a SPN elicited by ChAT interneurons were blocked by DHβE (red traces). *Bottom:* Cell attached recording demonstrated long latency spikes in a ChAT interneuron (arrows) coinciding with late inhibition. Note that the early inhibition is elicited by other ChAT interneurons.

Author Manuscript Author Manuscript Author Manuscript Author Manuscript

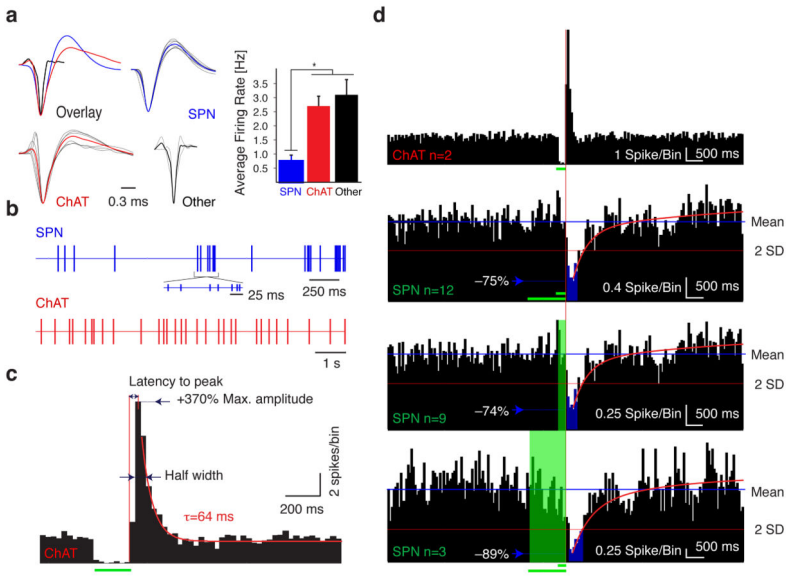

Figure 6. Pause-excitation sequences of ChAT interneurons inhibit SPNs *in vivo* in freely moving mice

a. *Left*: Waveforms of distinct types of units included in analysis. Average unit waveform is shown in gray, population averages are in color. Overlay demonstrates feature differences between unit types. *Right*: Firing rates (mean±s.e.m) of the 3 type of units. SPNs exhibit significantly lower firing rates than other unit types (t-test, $p<0.01$).

b. Examples of spike trains of putative SPNs and ChAT interneurons. Note that a bursting episode was selected for the SPN.

c. Characteristics of the population response of ChAT interneurons elicited with optogenetic inhibition. Note the instantaneous inhibition of firing and the excitation phase that is similar to responses of putative ChAT interneurons in primates (bins, 30 ms).

d. Inhibition of firing of SPNs (bottom 3 PSTHs) by pause-excitation activity pattern of ChAT interneurons (top). Lower 3 PSTHs show (respectively, from top to bottom) cumulative response of all SPNs, SPN responses following 200 ms optical inhibition and responses following 1000 ms inhibition. The population mean and mean-2SD firing rates are indicated by blue and red lines, respectively. Note that the end of the optical stimulus is closely followed by strong inhibition of firing in SPNs. Consecutive bins with firing rates below mean-2SD are indicated by bins colored in blue. Note that the optical inhibition itself does not elicit statistically significant firing rate changes in the SPNs. Horizontal bars denote periods of illumination (bins, 50 ms).